A new phase-shifted long-period fiber grating for simultaneous measurement of torsion and temperature

Cuiting Sun (孙翠婷)[1], Ran Wang (王冉)[1], Xiren Jin (金夕人)[1], Zemin Wang (王泽民)[1], Weiliang Liu (刘卫亮)[1], Shuo Zhang (张硕)[1], Yiwei Ma (马一巍)[1], Jingyu Lin (林静雨)[1], Yue Li (李 玥)[1], Tao Geng (耿 涛)[1,*], Weimin Sun (孙伟民)[1,], Zhongquan Qu (屈中权)[2], and Libo Yuan (苑立波)[3]**

[1]*Key Laboratory of In-Fiber Integrated Optics, Ministry of Education, Harbin Engineering University, Harbin 150001, China*

[2]*Yunnan Observatories, Chinese Academy of Sciences, Kunming 650216, China*

[3]*Photonics Research Center, Guilin University of Electronics Technology, Guilin 541004, China*

**Corresponding author: gengtao_hit_oe@126.com; **corresponding author: sunweimin@hrbeu.edu.cn*

Received September 16, 2019; accepted November 7, 2019; posted online January 6, 2020

A novel phase-shifted long-period fiber grating (PS-LPFG) for the simultaneous measurement of torsion and temperature is described and experimentally demonstrated. The PS-LPFG is fabricated by inserting a pre-twisted structure into the long-period fiber grating (LPFG) written in single-mode fiber (SMF). Experimental results show that the torsion sensitivities of the two dips are −0.114 nm/(rad/m) and −0.069 nm/(rad/m) in the clockwise direction, and −0.087 nm/(rad/m) and −0.048 nm/(rad/m) in the counterclockwise direction, respectively. The temperature sensitivities of the two dips are 0.057 nm/°C and 0.051 nm/°C, respectively. The two dips of the PS-LPFG exhibit different responses to torsion and temperature. Simultaneous measurement of torsion and temperature can be implemented using a sensor. The feasibility and stabilization of simultaneous torsion and temperature measurement have been confirmed, and hence this novel PS-LPFG demonstrates potential for fiber sensing and engineering applications.

Keywords: phase-shifted long-period fiber grating; pre-twisted structure; single-mode fiber; simultaneous measurement; torsion; temperature.

doi: 10.3788/COL202018.021203.

Torsion is an important physical parameter that has been used to monitor the condition of bridges and buildings. Among numerous torsion sensing technologies, optical fiber torsion sensors possess intrinsic merits of the simple fabrication process, compact size, easy integration, high sensitivity, and immunity to electromagnetic interference[1]. Over the past few decades, many torsion sensors based on fiber Bragg gratings (FBGs)[2,3], fiber interferometers[4,5], and long-period fiber gratings (LPFGs)[6–10] have been studied. Torsion sensors can involve diverse fiber structures such as the helical structure[11], near-helical structure[12], pre-twisted structure[13], and twisted photonic crystal fiber[14,15]. A sensor based on a CO_2 laser-written LPFG can discriminate the torsion direction due to a unique one-sided laser exposure method. Torsion sensors with a pre-twisted structure exhibit high sensitivity because of permanent shear strain in the structure. However, the performance of torsion sensors could be affected by temperature. To eliminate the cross talk effect, one approach involves the simultaneous measurement of torsion and temperature. Many researchers have used different structures to measure torsion and temperature simultaneously. For instance, Li *et al.* reported a novel sensor by combining a helically twisted fiber and a Bragg grating[16], Wang *et al.* fabricated a fiber loop mirror based on a piece of homemade side-leakage photonic crystal fiber[17], Shao *et al.* manufactured a Lyot–Sagnac interferometer by inserting two sections of high-birefringence (HiBi) fiber into a Sagnac loop[18], and Zhang *et al.* proposed a Mach–Zehnder interferometer based on multicore fiber with a ~570 μm long helical structure[19] for application in the simultaneous torsion and temperature measurement. However, the above sensors display some certain shortcomings. For example, fiber interferometers are relatively complex structures, and the fabrication of special fibers is costly and somewhat complicated. Thus, a simple and inexpensive method is needed to fabricate a sensor capable of the simultaneous measurement of torsion and temperature.

A phase-shifted long-period fiber grating (PS-LPFG) can be used as a fiber sensor to measure torsion and temperature simultaneously because of the advantages including dual-transmission peaks, high sensitivity, and easy fabrication. But the pre-twisted structure used in a PS-LPFG has not yet been proposed as a sensor for the simultaneous measurement of torsion and temperature.

In this study, we design a novel PS-LPFG to measure torsion and temperature simultaneously. This PS-LPFG is manufactured by inserting a pre-twisted structure into the LPFG. The pre-twisted structure is fabricated via filament heating, and the LPFG is written in single-mode fiber (SMF) using a high-frequency CO_2 laser. The proposed sensor can also discriminate the torsion direction and improve torsion sensitivity.

Fabrication of the proposed PS-LPFG consists of two processes: pre-twisted structure fabrication and writing the grating. First, the SMF was mounted onto two fiber holders, one fixed and the other rotatory. A supercontinuum light source (SLS) with a spectrum range of 600–1700 nm and an optical spectrum analyzer (OSA) were placed on both sides of the fiber to record transmission spectra, as shown in Fig. 1. The fiber structure was continuously rotated using the rotatable fiber holder, after which the filament heater heated the SMF and a pre-twisted structure was finished. An irreversible twist was formed after heating. The length of the structure was L_0 ($L_0 > 1$ mm), determined by the fixed size of the filament heater and the fabrication technology. Twisting process parameters were carefully optimized to ensure minimal transmission loss[20]. The experimental parameters are listed in Table 1. Second, the pre-twisted structure was placed in the center of the preparation area via CCD monitoring, and the grating was written by exploiting a high-frequency CO_2 laser (CO2-H10, Han's Laser) under computer control. Transmission spectra were monitored by an SLS and an OSA, as depicted in Fig. 2. The LPFG period was Λ ($\Lambda = 500$ μm) and the PS-LPFG length was 2.45 cm, as indicated in Fig. 3.

When the pre-twisted structure is inserted into the LPFG, the original transmission peak of the LPFG is split into two. The equivalent phase-shift inserted into the LPFG can be approximated as[21]

$$\Phi = \frac{2\pi}{\lambda} \cdot L_0\left(n_{\text{eff}}^{\text{core}} - n_{\text{eff}}^{\text{clad}}\right), \tag{1}$$

where $\lambda = \Lambda \cdot (n_{\text{eff}}^{\text{core}} - n_{\text{eff}}^{\text{clad}})$ is the central wavelength, L_0 is the length of the pre-twisted structure, and $\Delta n_{\text{eff}} = n_{\text{eff}}^{\text{core}} - n_{\text{eff}}^{\text{clad}}$ is the difference between effective refractive indices of the core and cladding modes. According to Eq. (1), the phase shift introduced in the structure depends on L_0 and Δn_{eff}.

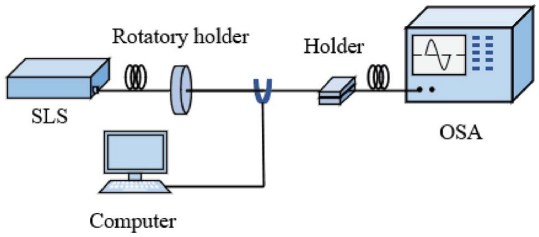

Fig. 1. Experimental setup for fabricating the pre-twisted structure.

Table 1. Experimental Parameters for Fabricating the Pre-twisted Structure

Parameter	Data	Unit
Heating temperature	1300 ± 20	°C
Heating time	10	s
Heating length	1	mm
Number of twisting turns	15	1

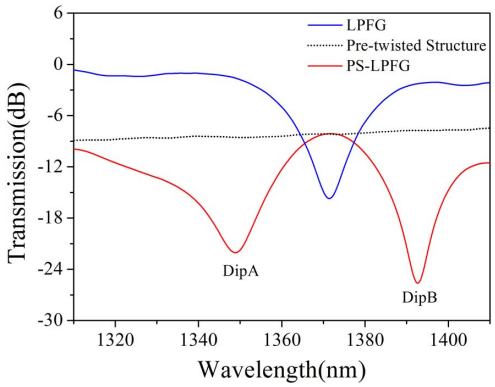

Fig. 2. Transmission spectra of the pre-twisted structure, LPFG, and PS-LPFG.

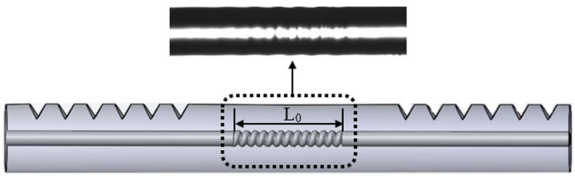

Fig. 3. Structure diagram of the PS-LPFG.

The PS-LPFG induces a permanent twist strain in the fused twist process. As for the twist turn in the pre-twisted structure, with an increase in the twisting turn (N), the initial twist strain of the PS-LPFG increases. When torsion is applied to the sensor, according to $\lambda = \Lambda \cdot \Delta n_{\text{eff}}$, the wavelength shift $\Delta\lambda$ can be derived as[22]

$$\Delta\lambda \approx \lambda \frac{\delta\Delta n_{\text{eff}}}{\Delta n_{\text{eff}}}, \tag{2}$$

where $\delta\Delta n_{\text{eff}}$ is the variable of Δn_{eff}, which is induced by birefringence resulting from the photoelastic effect. $\delta\Delta n_{\text{eff}}$ in response to the torsion rate τ can be expressed as

$$\delta\Delta n_{\text{eff}} = \left(g^{\text{core}} n_{\text{eff}}^{\text{core}} - g^{\text{clad}} n_{\text{eff}}^{\text{clad}}\right)\tau, \tag{3}$$

where g^{core} and g^{clad} denote photoelastic constants for the fiber core and cladding material, respectively. Therefore, the following equation can be obtained by substituting Eq. (3) into Eq. (2):

$$\begin{aligned}\Delta\lambda &= \frac{\lambda}{\Delta n_{\text{eff}}}\left(g^{\text{core}} n_{\text{eff}}^{\text{core}} - g^{\text{clad}} n_{\text{eff}}^{\text{clad}}\right)\tau \\ &= \frac{K\lambda}{\Delta n_{\text{eff}}}\tau = T\tau.\end{aligned} \tag{4}$$

From Eq. (4), T is a wavelength-independent constant; thus, the wavelength shift is linearly proportional to the torsion rate. For the proposed PS-LPFG, the pre-twisted structure induced a permanent twist strain. The value of

N directly affects the twist strain in the sensor, so the larger N will cause more obvious changes of wavelength, and it also means a greater torsion sensitivity. However, if N is too large, then insertion loss can also be excessive; considering insertion loss and torsion sensitivity, a suitable N is thus determined as 15. When the PS-LPFG is twisted in a clockwise or counterclockwise direction, $\delta\Delta n_{\text{eff}}$ will be either enhanced or impaired. Therefore, the proposed structure can discriminate the torsion direction. When the ambient temperature changes, the resonance wavelength shifts. Due to distinct cladding modes with different sensitivities toward torsion and temperature, the PS-LPFG can be utilized for the simultaneous measurement of torsion and temperature by evaluating the wavelength shift of two dips.

Figure 4 illustrates the measurement setup for torsion and temperature. Two disks fixed the structure and one was employed to change the torsion rate of the sensor. The distance between two disks was L ($L = 21$ cm). An SLS and an OSA with a resolution of 0.02 nm were employed to record the transmission spectrum. Meanwhile, the sensor was independently heated between the two disks by the heating device.

Figure 5 presents the transmission spectra corresponding to different torsion rates in two torsion directions. The applied torsion rate is $\tau = \theta/L$ (θ represents the torsion angle). When the τ range is from 0 to 8.308 rad/m in the clockwise direction, the resonance wavelength of the two dips exhibits a blue shift. When the τ range is from 0 to −8.308 rad/m in the counterclockwise direction, the resonance wavelength of the two dips exhibits a red shift. The linearity of the data is quite good; the linear fitting of the PS-LPFG wavelengths under different torsion rates is shown in Fig. 6. Torsion sensitivities of the two dips are −0.114 nm/(rad/m) and −0.069 nm/(rad/m) in the clockwise direction, and −0.087 nm/(rad/m) and −0.048 nm/(rad/m) in the counterclockwise direction, respectively.

The temperature characteristic of the PS-LPFG has been studied experimentally. Changes in transmission spectra of the PS-LPFG under different temperatures are shown in Fig. 7. When the applied temperature shifts from 40 to 100°C with a step of 10 °C, the wavelengths of the two dips shift from 1349.50 to 1352.95 nm and from 1393.05 to 1396.10 nm, respectively. Close linear correlations are observed between the wavelength and temperature of the two dips, as shown in Fig. 8. It can be seen that the respective temperature sensitivities of two dips are 0.057 nm/°C and 0.051 nm/°C.

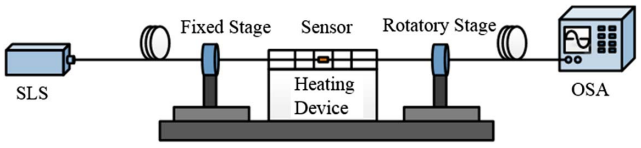

Fig. 4. Experimental setup for torsion and temperature measurement.

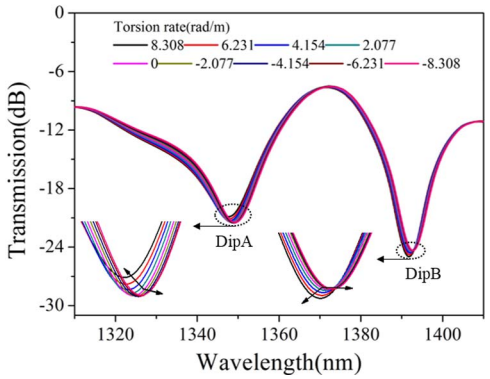

Fig. 5. Transmission spectra of the PS-LPFG under different torsion rates.

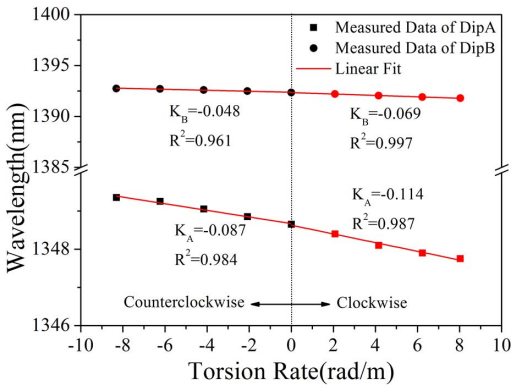

Fig. 6. Wavelength of the PS-LPFG versus torsion rate.

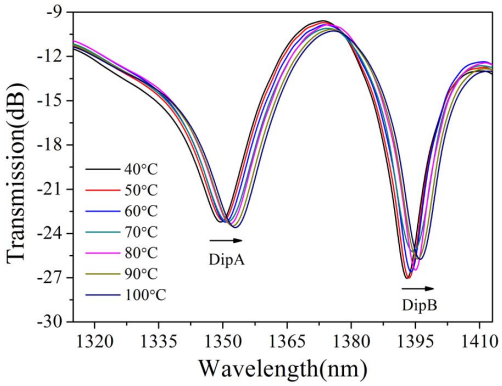

Fig. 7. Transmission spectra of the PS-LPFG under different temperatures.

The above experimental results reveal that the two dips respond differently to torsion and temperature. Simultaneous torsion and temperature measurements can be realized by detecting the wavelength shift of two dips. Due to the pre-twisted structure inserted into the LPFG, the torsion sensitivities of the sensor can be distinguished in the clockwise and counterclockwise directions, producing a matrix in each torsion direction. The simultaneous measurement matrices of the PS-LPFG can be expressed as[23]

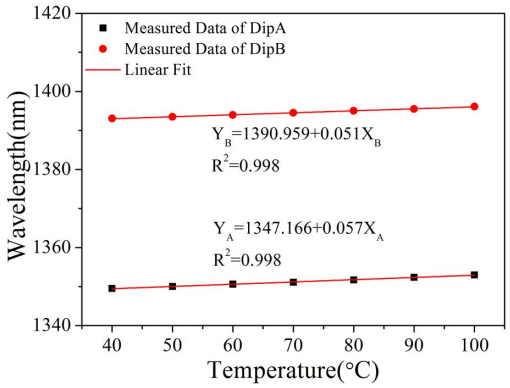

Fig. 8. Resonance wavelength of the PS-LPFG responding to temperature.

$$\begin{pmatrix} \Delta\tau \\ \Delta T \end{pmatrix}_C = \begin{pmatrix} -0.114 & 0.057 \\ -0.069 & 0.051 \end{pmatrix}^{-1} \begin{pmatrix} \Delta\lambda_A \\ \Delta\lambda_B \end{pmatrix}, \quad (5)$$

$$\begin{pmatrix} \Delta\tau \\ \Delta T \end{pmatrix}_{C-C} = \begin{pmatrix} -0.087 & 0.057 \\ -0.048 & 0.051 \end{pmatrix}^{-1} \begin{pmatrix} \Delta\lambda_A \\ \Delta\lambda_B \end{pmatrix}. \quad (6)$$

In this experiment, the resonance wavelength resolution of the OSA is 0.02 nm. From Eqs. (5) and (6), the torsion and temperature resolutions of the sensor are 0.063 rad/m and 0.5°C in the clockwise direction, and 0.071 rad/m and 0.5°C in the counterclockwise direction, respectively.

To evaluate the feasibility and stabilization of the simultaneous measurement of torsion and temperature, torsion experiments have been performed under different temperatures. In these experiments, the torsion rate ranges from 8.308 to −8.308 rad/m, and the temperature ranges from 40 to 100°C. Experimental results appear in Fig. 9. Standard deviations of torsion and temperature sensitivities are small, suggesting a negligible cross talk effect between torsion and temperature. Therefore, stabilization and feasibility are demonstrated when using the PS-LPFG to measure torsion and temperature simultaneously.

In summary, a new type of PS-LPFG has been presented to measure torsion and temperature simultaneously. The PS-LPFG is fabricated by inserting a pre-twisted structure into the LPFG. The LPFG is written in SMF via the CO_2 laser engraving method. Experimental results show that the torsion sensitivities of the two dips are −0.114 nm/(rad/m) and −0.069 nm/(rad/m) in the clockwise direction, and −0.087 nm/(rad/m) and −0.048 nm/(rad/m) in the counterclockwise direction, respectively. The sensor can also discriminate between the torsion direction and torsion rate. The temperature sensitivities of the two dips are 0.057 nm/°C and 0.051 nm/°C, respectively. Torsion resolutions of the PS-LPFG are estimated to be approximately 0.063 rad/m and 0.071 rad/m in the clockwise and counterclockwise directions, respectively, and the temperature resolution of the PS-LPFG is 0.5°C. The feasibility and stabilization of

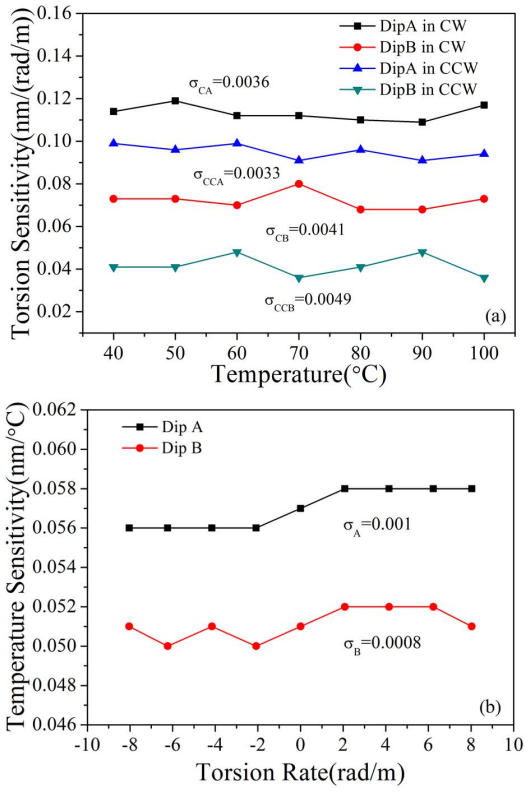

Fig. 9. Simultaneous measurement of torsion and temperature results. (a) Torsion sensitivities of the PS-LPFG under different temperatures. (b) Temperature sensitivities of the PS-LPFG under different torsion rates.

simultaneous torsion and temperature measurement using the proposed structure are thus demonstrated through the experimental process. Therefore, the PS-LPFG demonstrates encouraging prospects for sensing applications.

This work was supported by the National Natural Science Foundation of China (No. 11527804), Joint Research Fund in Astronomy under cooperative agreement between the National Natural Science Foundation of China (NSFC) and Chinese Academy of Sciences (CAS) (Nos. U1831115 and U1631239), Open Project of Key Laboratory of Astronomical Optics & Technology, Nanjing Institute of Astronomical Optics & Technology, Chinese Academy of Sciences (No. CAS-KLAOT-KF201806), Fundamental Research Funds for the Central Universities, and 111 Project (No. B13015) at the Harbin Engineering University.

References

1. Y. P. Li, L. Chen, Y. X. Zhang, W. G. Zhang, S. Wang, Y. S. Zhang, T. Y. Yan, W. Hu, X. Y. Li, and P. C. Geng, Opt. Express **25**, 13448 (2017).
2. C. Y. Shen, Y. Zhang, W. J. Zhou, and J. Albert, Appl. Phys. Lett. **104**, 071106 (2014).
3. Q. Liu, B. Zhang, Q. Chai, Y. Tian, Y. L. Liu, J. Ren, C. Liu, J. Z. Zhang, E. Lewis, W. P. Zhang, S. Wang, Z. H. Liu, J. Yang, and L. B. Yuan, IEEE Photon. Technol. Lett. **30**, 654 (2018).

4. Y. Chen, Y. Semenova, G. Farrell, F. Xu, and Y. Q. Lu, IEEE Photon. Technol. Lett. **27**, 2579 (2015).
5. C. Liu, Y. J. Jiang, B. B. Du, T. Wang, D. Y. Feng, B. Q. Jiang, and D. X. Yang, Sens. Actuators A **290**, 172 (2019).
6. X. R. Dong, Z. Xie, Y. X. Song, K. Yin, Z. Luo, J. Duan, and C. Wang, Opt. Laser Technol. **97**, 248 (2017)
7. Z. J. Zhang, W. K. Shi, K. Gao, and Z. J. Fang, Chin. Opt. Lett. **2**, 565 (2004).
8. R. Gao, Y. Jiang, and L. Jiang, Opt. Express **22**, 15697 (2014).
9. M. Deng, J. S. Xu, Z. Zhang, Z. Y. Bai, S. Liu, Y. Wang, Y. Zhang, C. R. Liao, W. Jin, G. D. Peng, and Y. P. Wang, Opt. Express **25**, 14308 (2017).
10. J. F. Xing, J. X. Wen, J. Wang, F. F. Pang, Z. Y. Chen, Y. Q. Liu, and T. Y. Wang, Chin. Opt. Lett. **16**, 100604 (2018).
11. H. L. Zhang, W. G. Zhang, L. Chen, Z. D. Xie, Z. Zhao, T. Y. Yan, and B. Wang, IEEE Photon. Technol. Lett. **28**, 1700 (2016).
12. Z. H. Han, C. T. Sun, X. R. Jin, H. Jiang, C. Yao, S. Zhang, W. L. Liu, T. Geng, F. Peng, W. M. Sun, and L. B. Yuan, Chin. Opt. Lett. **16**, 100601 (2018).
13. S. J. Duan, W. L. Liu, C. T. Sun, H. Jiang, C. Yao, K. Zhang, X. Y. Bai, W. Wang, C. L. Lu, T. Geng, F. Peng, and L. B. Yuan, IEEE Photon. J. **10**, 6804207 (2018).
14. F. Zhang, S. Liu, Y. Wang, Y. J. Huang, X. Z. Xu, C. L. Fu, T. S. Wu, C. R. Liao, and Y. P. Wang, Appl. Phys. Express **11**, 042501 (2018).
15. C. L. Fu, Y. P. Wang, S. Liu, Z. Y. Bai, J. Tang, L. P. Shao, and X. Y. Liu, Opt. Lett. **44**, 1984 (2019).
16. J. Li, G. Y. Chen, P. Ma, L. P. Sun, C. Wu, and B. O. Guan, Opt. Express **26**, 12903 (2018).
17. X. Wang, S. Q. Lou, X. Z. Sheng, and S. Liang, Infrared Phys. Technol. **76**, 603 (2016).
18. L. Y. Shao, X. P. Zhang, H. J. He, Z. Y. Zhang, X. H. Zou, B. Luo, W. Pan, and L. S. Yan, Sensors **16**, 1774 (2016).
19. H. L. Zhang, Z. F. Wu, P. P. Shum, X. G. Shao, R. X. Wang, X. Q. Ding, S. N. Fu, W. J. Tong, and M. Tang, Opt. Express **26**, 544 (2018).
20. K. Tian, Y. F. Xin, W. L. Yang, T. Geng, J. Ren, Y. X. Fan, G. Farrell, E. Lewis, and P. F. Wang, J. Lightwave Technol. **35**, 1725 (2017).
21. X. L. Li, W. G. Zhang, L. Chen, and T. Y. Yan, IEEE Photon. Technol. Lett. **27**, 1946 (2015).
22. Z. Y. Bai, M. Deng, S. Liu, Z. Zhang, J. S. Xu, J. Tang, Y. Wang, C. R. Liao, and Y. P. Wang, IEEE Photon. J. **9**, 7103708 (2017).
23. X. Y. Jiang, P. Lu, Y. Sun, H. Liao, D. M. Liu, J. S. Zhang, and H. Liao, Chin. Opt. Lett. **16**, 040602 (2018).